Hot forming of Composite prepreg: Numerical analyses

Eduardo Guzman-Maldonado, Nahiene Hamila, Philippe Boisse, Khalid El Azzouzi, Xavier Tardif, Tanguy Moro, Sylvain Chatel, Paulin Fideu

Hot forming of Composite prepreg: Numerical analyses

Eduardo GUZMAN-MALDONADO[1,a)], Nahiène HAMILA[2, b)], Philippe BOISSE[2,c)], Khalid EL AZZOUZI[1, d)], Xavier TARDIF[1)], Tanguy MORO[1)], Sylvain CHATEL[3)], Paulin FIDEU[4)]

[1]*IRT Jules Verne, Centre Technocampus EMC2, Chemin du Chaffault, 44340 Bouguenais, France*
[2]*University of Lyon, INSA-Lyon, LaMCos, F-69621 Lyon, France*
[3]*AIRBUS Group Innovations, Centre Technocampus EMC2, Chemin du Chaffault, 44340 Bouguenais, France*
[4]*AIRBUS Civil Aircraft, Germany*

[a)] Corresponding author: eduardo.guzman-maldonado@irt-jules-verne.fr
[b)] nahiene.hamila@insa-lyon.fr
[c)] philippe.boisse@insa-lyon.fr
[d)] khalid.el-azzouzi@irt-jules-verne.fr

Abstract. The work presented here is part of the "FORBANS" project about the Hot Drape Forming (HDF) process consisting of unidirectional prepregs laminates. To ensure a fine comprehension of this process a combination strategy between experiment and numerical analysis is adopted. This paper is focused on the numerical analysis using the finite element method (FEM) with a hyperelastic constitutive law. Each prepreg layer is modelled by shell elements. These elements consider the tension, in-plane shear and bending behaviour of the ply at different temperatures. The contact/friction during the forming process is taken into account using forward increment Lagrange multipliers.

INTRODUCTION

To unsure the reducing of the aircraft weight in the aeronautic industry, the composite components are used due to their light weight, high stiffness and high strength and have seen increased use in the couple of decades. The pr-impregnated carbon fibre (prepreg) is the dominating material used in the manufacturing process of aircraft components.

The fact that the use of prepreg increases by growing interest leads to increasing the drive to automate the manufacturing processes. Among the automated processes for lay-up and forming prepreg, we can list Automatic Tape Laying (ATL), Advanced Fiber Placement (AFP) and Hot Drape Forming (HDF). The last one is the process which studied in this paper and is classified as a thermoset prepreg forming process with the characteristic of long time polymerization after forming. The forming process must be performed at a temperature close to or higher than the melt temperature of the resin renders the unidirectional reinforcement deformation possible.

The quality of the shape manufacturing using inflatable bladder depends to the geometric of the final composite parts, on the reinforcement type and orientation (UD, properties of fibre and resin…) and on manufacturing parameters (tool and inflatable bladder loads, temperature…). Several software tools for composites forming have been developed to study the process feasibility and optimize the main forming parameters [1,2]. The present paper presents an extension of the software that has been developed for the simulations of the forming of dry textile reinforcements that are used in LCM processes [3]. It presents numerical simulation analysis of continuous fibre reinforcements with thermoplastic resin composites forming taken into account thermal and viscous effects.

These software packages need the mechanical behaviours of the composite ply during forming. As this ply is generally modelled by shell finite elements (or membrane elements if the bending stiffness is neglected), the mechanical behaviour of the prepreg ply during forming is given by the biaxial tensile properties [4,5], the in-plane shear properties [6–9] and the bending properties [10]. The simple axial tensile test gives the mechanical parameters

of fibre and the bending stiffness is very low because of the possible motion between the fibres. In-plane shear is the most important deformation mode [11].

NUMERICAL MODELLING

Modelling and numerical simulation of these processes is an important step in order to predict the final structure geometry and its mechanical properties which are mainly due to the position of the fibre reinforcements in the final configuration. Forming simulation allows to determine the feasibility conditions of the structure and optimize the process.

The numerical modelling of unidirectional composites forming can be realized at different scales as textile composites, which are specific and complex due to the interactions and the possible motions between fibres [12] or yarns [13] or lay-up [2,14]. A large number of continuous mechanical models have been proposed for the simulation of prepregs composite forming [15–20]. However, (here is no widely accepted model that accurately describes all aspects of the mechanical behaviour of fabrics.

In this paper a nonlinear visco-hyperelastic model is used for the simulation of thermoforming UD prepreg composites. This model is based on a recent proposed model developed for the simulation of prepreg thermoplastic woven composites [20,21]. The hyperelastic behaviour is associated to the dry reinforcement and it assumes that the viscoelastic behaviour is mainly associated with the in-plane shear deformation.

Anisotropic visco-hyperelastic constitutive model

The composite reinforcement is considered to be an orthotropic material in the initial configuration. Three privileged directions can be defined: $\underline{L}_1$ oriented in fibre directions, $\underline{L}_2$ perpendicular to $\underline{L}_1$, and $\underline{L}_3$ orthogonal to the plane defined by $\underline{L}_1$ and $\underline{L}_2$. This allows to define the structural tensors to characterise the physical symmetry group of the material [22]:

$$L_{ij} = L_i \otimes L_j \quad i,j = 1,2,3 \tag{1}$$

The internal potential energy of the material in the initial configuration is given by the addition of the membrane and bending energy contributions.

$$w^{UD} = w^{mem} + w^{ben} \tag{2}$$

The representation theorems [23], show that, for an orthotropic material, the strain energy density function of a hyperelastic law is of the form:

$$w^{orth} = w^{orth}\left(I_1, I_2, I_3, I_{41}, I_{42}, I_{412}, I_{423}, I_{51}, I_{52}, I_{53}\right) \tag{3}$$

Where $\underline{I}_1, \underline{I}_2, \underline{I}_3$ are the classic invariants of the right Cauchy-green tensor $\underline{\underline{C}}$ defined by:

$$I_1 = tr\left(\underline{\underline{C}}\right), \quad I_2 = \frac{1}{2}\left(tr\left(\underline{\underline{C}}\right)^2 - tr\left(\underline{\underline{C}}^2\right)\right) \quad \text{and} \quad I_1 = \det\left(\underline{\underline{C}}\right) \tag{4}$$

And the mixed invariants:

$$I_{4i} = \underline{\underline{C}} : \underline{\underline{L}}_{ii}, \quad I_{4ij} = \underline{\underline{C}} : \underline{\underline{L}}_{ij} \quad \text{and} \quad I_{5i} = \underline{\underline{C}}^2 : \underline{\underline{L}}_{ii} \tag{5}$$

The specific nature of composite reinforcements leads to the assumption that the membrane contribution of each deformation mode is independent from the others [24,25]. The membrane strain energy potential is written as a function of three physical invariants associated with three principal deformation modes: extensions in the $\underline{L}_1$ and $\underline{L}_2$ directions and the in-plane shear deformation mode (fig. 1). Each physical invariant is a combination of the classical invariants (Eq.4 and Eq.5) and are based on physical observations of the UD prepreg.

As a result the strain energy density is the sum of each specific strain energy:

$$w^{UD} = w^{memb}\left(I_{elong_1}, I_{elong_2}, I_{shear}\right) + w^{ben} = w^{elong_1}\left(I_{elong_1}\right) + w^{elong_2}\left(I_{elong_2}\right) + w^{shear}\left(I_{shear}\right) + w^{ben}\left(I_{\chi_1}, I_{\chi_2}\right) \tag{6}$$

Where I_{χ_1} and I_{χ_2} denote the invariants associated with the bending deformation in the fibres directions ($\underline{L}_1$) and the transverse direction ($\underline{L}_2$).

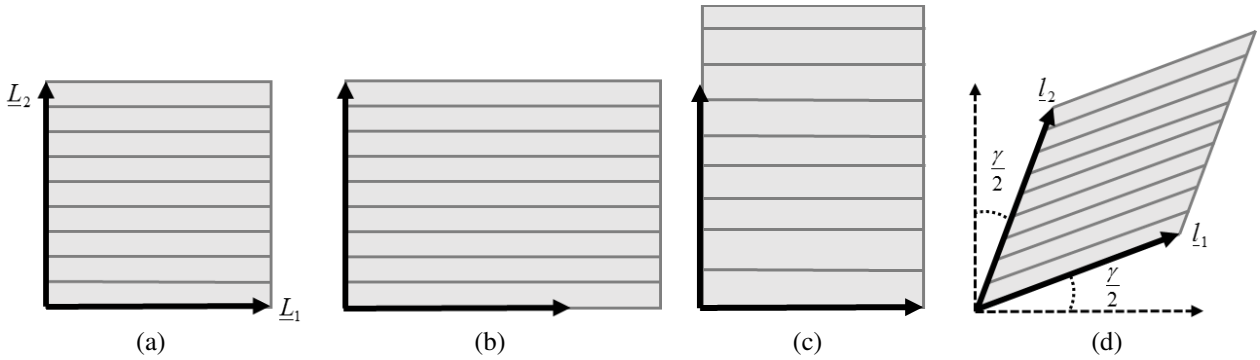

FIGURE 1. Deformation modes of UD reinforcement: (a) Initial configuration (b) Extension in fibres direction (c) Transverse extension (d) In-plane shear

The viscoelastic behaviour is introduced in the model introduced based on the generalization of the rheological Maxwell model and applying the concept of internal variables. It is assume that viscoelastic behaviour is mainly observed in-plane shear deformation. The second Piola-Kirchhoff stress tensor $\underline{\underline{S}}$ is given by the following expression:

$$\underline{\underline{S}} = 2\frac{\partial w^{mem}}{\partial \underline{\underline{C}}} - \sum_{i=1}^{N} \underline{\underline{Q}}_i = 2\frac{\partial w^{elong1}}{\partial I_{elong1}} \cdot \frac{\partial I_{elong1}}{\partial \underline{\underline{C}}} + 2\frac{\partial w^{elong2}}{\partial I_{elong2}} \cdot \frac{\partial I_{elong2}}{\partial \underline{\underline{C}}} + 2\frac{\partial w^{shear}}{\partial I_{shear}} \cdot \frac{\partial I_{shear}}{\partial \underline{\underline{C}}} - \sum_{i=1}^{N} \underline{\underline{Q}}_i \tag{7}$$

Or

$$\underline{\underline{S}} = \underline{\underline{S}}^{elong1} + \underline{\underline{S}}^{elong2} + \underline{\underline{S}}^{shear} \tag{8}$$

Where $\underline{\underline{S}}^{elong1}$ and $\underline{\underline{S}}^{elong2}$ are the purely hyperelastic contributions associated with the elongations in the $\underline{L}_1$ and $\underline{L}_2$ directions:

$$\underline{\underline{S}}^{elongi} = 2\frac{\partial w^{elongi}}{\partial I_{elongi}} \cdot \frac{\partial I_{elongi}}{\partial \underline{\underline{C}}} \quad i = 1,2 \tag{9}$$

And $\underline{\underline{S}}^{shear}$ is the in-plane shear visco-hyperelastic contribution which involves a set of internal variables $\underline{\underline{Q}}_i$ none directly measurable.

$$\underline{\underline{S}}^{shear} = 2\frac{\partial w^{shear}}{\partial I_{shear}} \cdot \frac{\partial I_{shear}}{\partial \underline{\underline{C}}} - \sum_{i=1}^{N} \underline{\underline{Q}}_i \tag{10}$$

The evolution of the internal variables is given by:

$$\underline{\underline{Q}}_i = \frac{\gamma_i}{\tau_i} \int_{-\infty}^{t} \exp\left(\frac{-(t-s)}{\tau_i}\right) \left[2\frac{\partial w^{shear}}{\partial \underline{\underline{C}}}\right] \mathrm{ds} \tag{11}$$

T involves the definition of material parameters $\gamma_i \in [0,1[$ associated with the relaxation times τ_i. All the parameters of the present stress contribution depend on the temperature (w^{shear}, γ_i and τ_i). They are assumed to be piecewise linearly dependent on the temperature.

Finally, the bending moments are given by:

$$M_{ii} = \frac{1}{J}\frac{\partial w^{ben}}{\partial I_{\chi_i}} \quad i = 1,2 \tag{12}$$

J being the radio between the current and the initial surfaces.

The identification of viscoelastic parameters is performed using the Levenberg–Marquardt algorithm [26] for fitting experimental results using the Picture Frame Test [7] at different temperatures. Bending parameters are identified using a cantilever test performed in an environmental chamber [27].

Surface contact management

In addition to the mechanical constitutive model, the contact phenomena between layers and with tools drive the thermo-mechanical behaviour of the U-D prepreg during the forming process. Four types of contact surface can be listed: point/point, point/surface, point/edge and edge/edge (fig. 2).

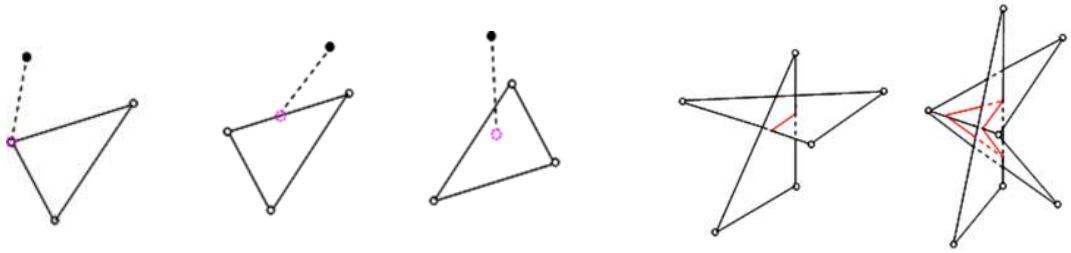

(a) node/node (b) node/edge c) node/surface (d) edge/edge

FIGURE 2. Different types of contact considered in the numerical model [28]

The numerical modelling of contact/friction behaviour during the forming process is accomplished using the algorithm of the forward increment Lagrange multipliers proposed by Carpenter et al. [29]. This method could be introduced into the dynamical expression (Eq. 14) as contact occurs.

$$\begin{aligned} &\underline{\underline{M}}\,\underline{\ddot{u}}_n + \underline{F}_n^{int} + \underline{\underline{G}}_{n+1}^{T}\,\underline{\lambda}_n = \underline{F}_n^{ext} \\ &\underline{\underline{G}}_{n+1}\left(\underline{u}_n + \underline{X}_0\right) = 0 \end{aligned} \tag{13}$$

Where $\underline{u}$ is the vector of displacement degrees of freedom, $\underline{X}_0$ is the material co-ordinate vector, $\underline{\underline{M}}$ is the mass matrix, $\underline{F}^{int}$ and $\underline{F}^{ext}$ are internal and external loads vectors of the system, $\underline{\lambda}_n$ is Lagrange multiplier vector and its components are slave nodal contact forces, n is an index of calculation step, $\underline{\underline{G}}$ is a surface contact displacement constraint matrix.

The Lagrange multiplier $\underline{\lambda}_n$ at each node can be calculated according to Eq.14 by a predictor $\underline{u}^*_{n+1}$ determined at the time n+1 from Eq.13 without contact conditions.

$$\underline{\lambda}_n = \frac{1}{\Delta t^2}\left(\underline{\underline{G}}_{n+1}\underline{\underline{M}}^{-1}\underline{\underline{G}}_{n+1}^{T}\right)^{-1}\underline{\underline{G}}_{n+1}\left(\underline{u}^*_{n+1} + \underline{X}_0\right) \tag{14}$$

The total displacement $\underline{u}_{n+1}$ at the time n+1 is now given by the addition of this predictor displacement and a corrector vector displacement $\underline{u}^c_{n+1}$.

$$\underline{u}^c_{n+1} = \Delta t^2\left(\underline{\underline{M}}^{-1}\underline{\underline{G}}_{n+1}^{T}\right)\underline{\lambda}_n \tag{15}$$

$$\underline{u}_{n+1} = \underline{u}^*_{n+1} + \underline{u}^c_{n+1} \tag{16}$$

Finite element discretization

This continuous model has been implemented in PlasFib®, an explicit finite element code developed by INSA Lyon [3,30], using a three node shell element without rotational degrees of freedom [31]. The curvatures of the element are computed from the position of the neighbour elements [3,31].

The numerical integration of Eq. 11 can be achieved through a recursive relation (two-step recursive formula) established by Simo an Hughes [32]. The update formula for the algorithmic internal variables $\underline{\underline{H}}_i$ at each integration point is given by:

$$\underline{\underline{H}}_i\left(t_{n+1}\right) = \exp\left(\frac{-\Delta t_n}{\tau_i}\right)\cdot\underline{\underline{H}}_i\left(t_n\right) + 2\cdot\exp\left(\frac{-\Delta t_n}{2\tau_i}\right)\left[\frac{\partial w^{shear}\left(I_{sh}\right)}{\partial \underline{\underline{C}}_{n+1}} - \frac{\partial w^{shear}\left(I_{sh}\right)}{\partial \underline{\underline{C}}_{n}}\right] \tag{17}$$

Where $\Delta t_n = t_{n+1} - t_n$ is the corresponding time increment.

ACKNOWLEDGMENTS

This study is part of the “FORBANS” project managed by IRT Jules Verne (French Institute in Research and Technology in Advanced Manufacturing Technologies for Composite, Metallic and Hybrid Structures). The authors wish to associate the industrial and academic partners of this project; Respectively Airbus, Airbus Group Innovations and LAMCOS (INSA of Lyon).

REFERENCES

1. P. de Luca, P. Lefebure, and A. K. Pickett, "Numerical and experimental investigation of some press forming parameters of two fibre reinforced thermoplastics: APC2-AS4 and PEI-CETEX," Compos. Part Appl. Sci. Manuf. **29**, 101–110 (1998).
2. R. H. W. ten Thije and R. Akkerman, "A multi-layer triangular membrane finite element for the forming simulation of laminated composites," Compos. Part Appl. Sci. Manuf. **40**, 739–753 (2009).
3. N. Hamila, P. Boisse, F. Sabourin, and M. Brunet, "A semi-discrete shell finite element for textile composite reinforcement forming simulation," Int. J. Numer. Methods Eng. **79**, 1443–1466 (2009).
4. S. Kawabata, M. Niwa, and H. Kawai, "The finite-deformation theory of plain-weave fabrics part I: the biaxial-deformation theory," J. Text. Inst. **64**, 21–46 (1973).
5. A. Willems, S. V. Lomov, I. Verpoest, and D. Vandepitte, "Optical strain fields in shear and tensile testing of textile reinforcements," Compos. Sci. Technol. **68**, 807–819 (2008).
6. A. G. Prodromou and J. Chen, "On the relationship between shear angle and wrinkling of textile composite preforms," Compos. Part A **28A**, 491–503 (1997).
7. G. B. McGuinness and C. M. Braidaigh, "Characterisation of thermoplastic composite in rombus-shear: the picture frame experiment," Compos. Part A **29A**, 115–132 (1998).
8. P. Harrison, M. J. Clifford, and A. C. Long, "Shear characterisation of viscous woven textile composites: a comparison between picture frame and bias extension experiments," Compos. Sci. Technol. **64**, 1453–1465 (2004).
9. J. Cao, R. Akkerman, P. Boisse, J. Chen, H. S. Cheng, E. F. de Graaf, J. L. Gorczyca, P. Harrison, G. Hivet, J. Launay, W. Lee, L. Liu, S. V. Lomov, A. Long, E. de Luycker, F. Morestin, J. Padvoiskis, X. Q. Peng, J. Sherwood, T. Stoilova, X. M. Tao, I. Verpoest, A. Willems, J. Wiggers, T. X. Yu, and B. Zhu, "Characterization of mechanical behavior of woven fabrics: Experimental methods and benchmark results," Compos. Part Appl. Sci. Manuf. **39**, 1037–1053 (2008).
10. E. de Bilbao, D. Soulat, G. Hivet, and A. Gasser, "Experimental study of bending behaviour of reinforcements," Exp. Mech. **50**, 333–351 (2010).
11. P. Boisse, B. Zouari, and J. L. Daniel, "Importance of in-plane shear rigidity in finite element analyses of woven fabric composite preforming," Compos. Part Appl. Sci. Manuf. **37**, 2201–2212 (2006).
12. D. Durville, "Simulation of the mechanical behaviour of woven fabrics at the scale of fibers," Int. J. Mater. Form. **3**, 1241–1251 (2010).
13. N. Naouar, E. Vidal-Salle, J. Schneider, E. Maire, and P. Boisse, "Meso-scale FE analyses of textile composite reinforcement deformation based on X-Ray computed tomography," Compos. Struct. **116**, 165–176 (2014).
14. N. Hamila, P. Boisse, F. Sabourin, and M. Brunet, "A semi-discrete shell finite element for textile composite reinforcement forming simulation," Int J Numer Methods Eng **79**, 1443–1466 (2009).
15. T. G. Rogers, "Rheological characterization of anisotropic materials," Composites **20**, 21–27 (1989).
16. S.-W. Hsiao and N. Kikuchi, "Numerical analysis and optimal design of composite thermoforming process," Comput. Methods Appl. Mech. Eng. **177**, 1–34 (1999).
17. P. Harrison, M. J. Clifford, A. C. Long, and C. D. Rudd, "Constitutive modelling of impregnated continuous fibre reinforced composites Micromechanical approach," Plast. Rubber Compos. **31**, 76–86 (2002).
18. W. R. Yu, F. Pourboghrat, K. Chung, M. Zampaloni, and T. J. Kang, "Non-orthogonal constitutive equation for woven fabric reinforced thermoplastic composites," Compos. Part Appl. Sci. Manuf. **33**, 1095–1105 (2002).
19. R. H. W. ten Thije, R. Akkerman, and J. Huétink, "Large deformation simulation of anisotropic material using an updated Lagrangian finite element method," Comput. Methods Appl. Mech. Eng. **196**, 3141–3150 (2007).
20. E. Guzman-Maldonado, N. Hamila, P. Boisse, and J. Bikard, "Thermomechanical analysis, modelling and simulation of the forming of pre-impregnated thermoplastics composites," Compos. Part Appl. Sci. Manuf. **78**, 211–222 (2015).

21. E. Guzman-Maldonado, N. Hamila, N. Naouar, G. Moulin, and P. Boisse, "Simulation of thermoplastic prepreg thermoforming based on a visco-hyperelastic model and a thermal homogenization," Mater. Des. **93**, 431–442 (2016).
22. Z. Quanshui and J. P. Boehler, "Tensor function representations as applied to formulating constitutive laws for clinotropic materials," Acta Mech Sin **10**, 336–348 (1994).
23. M. Itskov, "A generalized orthotropic hyperelastic material model with application to incompressible shells," Int J Numer Methods Eng **50**, 1777–1789 (2001).
24. Y. Aimene, B. Hagege, F. Sidoroff, E. Vidal-Sallé, P. Boisse, and S. Dridi, "Hyperelastic Approach for Composite Reinforcement Forming Simulations," Int. J. Mater. Form. **1**, 811–814 (2008).
25. A. Charmetant, J. G. Orliac, E. Vidal-Sallé, and P. Boisse, "Hyperelastic model for large deformation analyses of 3D interlock composite preforms," Compos. Sci. Technol. **72**, 1352–1360 (2012).
26. D. S. Schnur and N. Zabaras, "An inverse method for determining elastic material properties and a material interface," Int. J. Numer. Methods Eng. **33**, 2039–2057 (1992).
27. B. Liang, N. Hamila, M. Peillon, and P. Boisse, "Analysis of thermoplastic prepreg bending stiffness during manufacturing and of its influence on wrinkling simulations," Compos. Part A **67**, 111–122 (2014).
28. P. Wang, N. Hamila, and P. Boisse, "Thermoforming simulation of multilayer composites with continuous fibres and thermoplastic matrix," Compos. Part B Eng. **52**, 127–136 (2013).
29. N. J. Carpenter, R. L. Taylor, and M. G. Katona, "Lagrange constraints for transient finite element surface contact," Int. J. Numer. Methods Eng. **32**, 103–128 (1991).
30. *PlasFib* (INSAVALOR – SIREN 345038244, 2011).
31. F. Sabourin and M. Brunet, "Detailed formulation of the rotation-free triangular element S3 for general purpose shell analysis," Eng. Comput. **23**, 469–502 (2006).
32. G. A. Holzapfel and J. C. Simo, "A new viscoelastic constitutive model for continuous media at finite thermomechanical changes," Int. J. Solids Struct. **33**, 3019–3034 (1996).